Journal of Materials Chemistry C

Accepted Manuscript

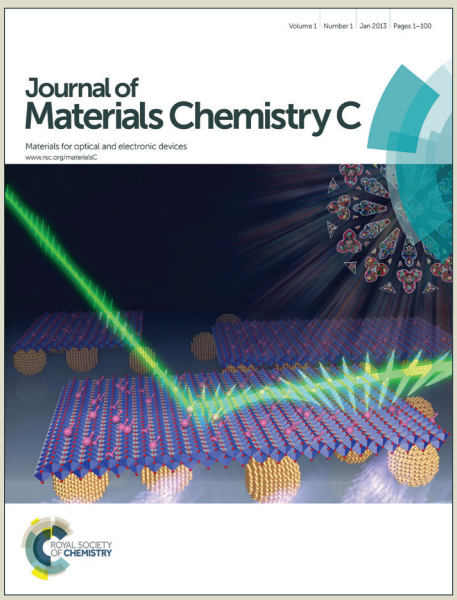

ROYAL SOCIETY OF CHEMISTRY

www.rsc.org/materialsC

ARTICLE TYPE www. rsc.org/xxxxxx | XXXXXXXX

Engineering electronic properties of Metal-$MoSe_2$ interfaces using self-assembled monolayers

Deniz Çakır,[*a] **Cem Sevik,**[b] **and François M. Peeters**[a]

Received Xth XXXXXXXXXX 20XX, Accepted Xth XXXXXXXXX 20XX
First published on the web Xth XXXXXXXXXX 200X
DOI: 10.1039/b000000x

Metallic contacts are critical components of electronic devices and the presence of a large Schottky barrier is detrimental for an optimal device operation. Here, we show by using first-principles calculations that a self-assembled monolayer (SAM) of polar molecules between the metal electrode and $MoSe_2$ monolayer is able to convert the Schottky contact into an almost Ohmic contact. We choose -CH_3 and -CF_3 terminated short-chain alkylthiolate (i.e. SCH_3 and fluorinated alkylthiolates (SCF_3)) based SAMs to test our approach. We consider both high (Au) and low (Sc) work function metals in order to thoroughly elucidate the role of the metal work function. In the case of Sc, the Fermi level even moves into the conduction band of the $MoSe_2$ monolayer upon SAM insertion between the metal surface and the $MoSe_2$ monolayer, and hence possibly switches the contact type from Schottky to Ohmic. The usual Fermi level pinning at the metal-transition metal dichalcogenide (TMD) contact is shown to be completely removed upon the deposition of a SAM. Systematic analysis indicates that the work function of the metal surface and the energy level alignment between the metal electrode and the TMD monolayer can be tuned significantly by using SAMs as a buffer layer. These results clearly indicate the vast potential of the proposed interface engineering to modify the physical and chemical properties of $MoSe_2$.

1 Introduction

The successful isolation of graphene has tremendously increased both scientific and technological interest on two dimensional (2D) materials[1–4]. Among them transition metal dichalcogenides (TMDs) as a large family of layered materials have particularly stood out due to their diverse electronic and magnetic properties ranging from semiconductor (such as MoS_2) to ferromagnetic metal (such as VS_2[5–12]). These ultrathin materials have been implemented in various technological applications including catalysis[11], energy storage[13], sensing[12], and electronic devices such as field-effect transistors[14–17] and logic circuits[7,12]. However, a detailed knowledge of the electronic properties of the interface between TMDs and metal electrodes, which is essential in order to implement TMDs in efficient device applications, is still lacking. Indeed, interfaces play a key role in the performance of a device constructed from low-dimensional materials because the injection, collection, concentration, and mobility of the charge carriers are mainly determined by the interfaces[18–23].

Recently, it was shown that at the metal-TMD interface a Schottky barrier appears due to the pinning of the Fermi level close to the conduction band of TMDs, resulting in a higher contact resistance which limited the carrier injection across the interface[18]. Fermi level pinning at the metal-TMD interface strongly determines the line up between the metal Fermi level and the valence or conduction band of TMD. A remedy to mitigate or to eliminate such Fermi level pinning at the interface was proposed by Chen *et al.*[24] and Dankert *et al.*[25] who demonstrated that the insertion of a thin oxide layer that acts as a tunnel barrier between the metal electrode and the TMD significantly lowers the Schottky barrier height. However, as an alternative, one can also control the Schottky barrier height and the energy level alignment (i.e., position of the metal Fermi level relative to either valence or conduction band edge of the TMD) at the interface by using self-assembled monolayers (SAMs) instead of oxides[26]. Depending on the detailed molecular composition and structure, the work function of a clean metal surface can be changed by several eVs using SAMs[27–34]. One of the key advantageous of using SAM in device applications is the existence of a large number of different types of molecules with distinctive physical and chemical properties and their large scale growth with minimal structural imperfections. In addition, the quite positive effect of the molecule buffer layers on the device performance was demonstrated in a recent study that reports that the multilayer $MoSe_2$ based FETs on parylene-C have a much larger room-temperature mobility (100-160 $cm^2/(Vs)$) than that on SiO_2 substrates ($\approx$ 50 $cm^2/(Vs)$[35].

In this study, we propose that the insertion of a SAM be-

[a] *Department of Physics, University of Antwerp, 2020 Antwerp, Belgium Fax: +32 3 265 3542; Tel: +32 3 265 3660; E-mail: deniz.cakir@uantwerpen.be*
[b] *Department of Mechanical Engineering, Faculty of Engineering, Anadolu University, Eskisehir, TR 26555, Turkey.*

tween a metal electrode and $MoSe_2$ has a large impact on the electronic structure at the interface such that the Schottky barrier height and hence the degree of *n*- or *p*- type doping of $MoSe_2$ can be tuned by the choice of a suitable molecule. The systematic calculations show that the *n*- or *p*-type characteristic of $MoSe_2$ can be significantly tuned by inserting different SAM monolayers. In particular, the vast potential of SAMs to be used as a buffer layer instead of oxides to tune the work function of metal surfaces and the energy level alignment between a metal electrode and a TMD monolayer is predicted in this study.

2 Methods

First principles plane wave calculations based on density functional theory are carried out by using the Vienna ab initio simulation package (VASP)[36,37] code using the GGA-PBE[38] functional to treat the electronic exchange correlation interaction. The projected augmented-wave (PAW) method is used to describe electron and ion interaction. Plane waves up to a kinetic energy cutoff of 400 eV are included in the calculations. For the structure optimizations, the Brillouin zone of the considered supercells shown in Fig. 1 and 6 is sampled by a 5×9 *k*-point mesh within Monkhorst-Pack scheme[39]. The density of state calculations are performed by using a 11×19 *k*-point mesh. To get accurate band structures, each high symmetry direction in the Brillouin zone is sampled by using 50 *k* points. The electronic relaxation convergence criteria and the maximum force allowed on each atom are chosen as 10^{-5} eV and 0.01 eV/Å, respectively. The Au(111) and Sc (0001) surfaces are modelled in a slab geometry containing four layers. The SAM is placed only on one side of the slab, and two bottom metal layers are kept frozen at their corresponding bulk positions. A vacuum region of at least 15 Å along the *z*-direction is used to separate the periodic images to avoid spurious interactions. In order to prevent interaction between the dipoles of repeated slabs, we include a dipole correction in the calculations. The work function (W) of each structure is obtained via $W = V(\infty)$-E_F , where $V(\infty)$ is the value of the electrostatic potential in vacuum, and E_F is the Fermi energy of the bulk metal. To obtain the electrostatic potential, and hence the potential drop at the metal/SAM interface, we calculate the plane averaged potential along the surface normal by using the following expression,

$$\overline{V}(z) = \frac{1}{A}\int\int_{cell} V(x,y,z)dxdy \qquad (1)$$

where A is the area of the surface unit cell. Since the semi-local functionals such as GGA fails to capture physisorption, we also take into account the van der Waals (vdW) interactions within the Grimme approach to provide a better description of the interfaces between the weakly interacting structures[40].

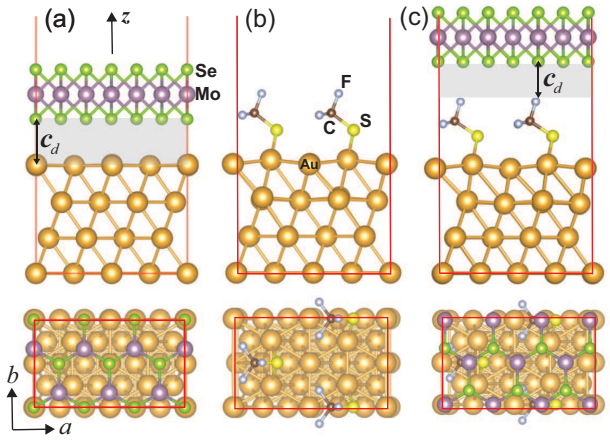

Fig. 1 (Color online) Optimized lowest energy structures: (a) $MoSe_2$ monolayer on Au (111) surface, (b) Au surface with SCF_3 SAM, and (c) $MoSe_2$ monolayer on the SAM covered Au surface. c_d, shown in (a), is the physical separation between the $MoSe_2$ monolayer and the pristine Au surface.

Since the VASP code does not include the C_6 parameter and the vdW radius for the Au atom, we use values given in the literature[41]. All the pair interactions up to a radius of 20 Å are included in the calculations. Another important point is the correct description of the energy level alignment at the interfaces of weakly interacting structures. To check the reliability of the results obtained by using GGA, we also performed calculations using a hybrid functional for the ground state structures calculated from GGA + vdW. We use the hybrid functional proposed by Heyd, Scuseria, and Ernzerhog (HSE06)[42–44]. While the short range part of the exchange interaction is modelled by a combination of GGA and Hartre-Fock in HSE06 functional, the long range part and the correlation interaction part are represented by the semi-local functional GGA.

3 Results

With the intention to clearly understand the effect of SAMs on the work function and on the interface electronic properties, metal|SAM|$MoSe_2$ structures are systematically investigated. To test the approach, SCH_3 and fluorinated alkylthiolates (SCF_3) SAMs are taken as examples due to their simple structure and the opposite intrinsic dipole moments, resulting in opposite changes in the work function of the metal surface. For metal electrode we consider both high (Au) and low (Sc) work function metals in order to thoroughly elucidate the role of the metal work function.

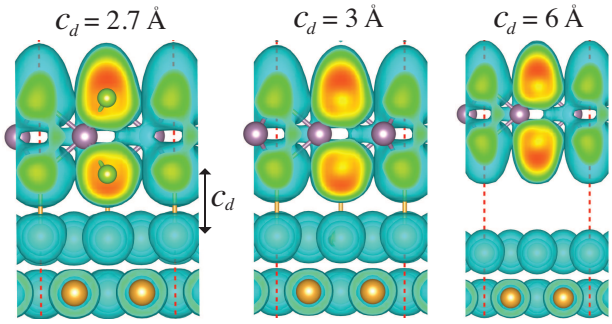

Fig. 3 (Color online) Electron localization function (ELF) plots for Au|$MoSe_2$ as a function of separation c_d.

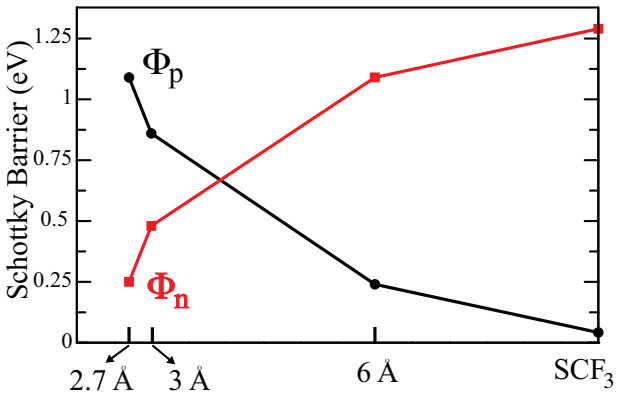

Fig. 4 (Color online) The calculated Schottky barrier heights in Au|$MoSe_2$ system for different interface separations and in Au|SCF_3|$MoSe_2$ system. Φ_p and Φ_n stand for the Schottky barriers for holes and electrons, respectively.

3.1 Au|SCF_3|$MoSe_2$

In order to clearly test our proposal regarding the tuning of Schottky barrier height and hence the degree of *n*- or *p*- type doping of $MoSe_2$, Au|$MoSe_2$, Au|SCF_3 and Au|SCF_3|$MoSe_2$ structures shown in Fig. 1 are considered. Previously, Rusu *et al.*[45] showed that adsorption of SCF_3 molecules on the Au (111) surface forms several structures with different packing densities, namely $(\sqrt{3}\times\sqrt{3})$R30°, c(4×2), and p(2×2). The authors also predicted that all those different structures result in a similar local geometry around the adsorbed molecules and in similar work function changes (ΔW). Therefore, among these possible structures the smallest and simplest p(2×2) is adopted in the present study for both metal surfaces. In order to fit the $MoSe_2$ monolayer on the metal surfaces with a tiny lattice mismatch (less than 0.5%), a rectangular unit cell is used in first principle calculations. The unit cell dimensions *a* and *b* are set to 11.47 (10.06) Å and 6.62 (5.81) Å for the Sc (Au) surface, respectively.

Table 1 shows the variation of ΔW as a function of the separation, c_d (which measures the distance between the bottom Se plane of $MoSe_2$ monolayer and the upmost layer of pure Au(111)/Sc(0001) or SAM covered Au(111)/Sc(0001) surfaces.). Definition of c_d is also denoted in Fig. 1 and 6. Similar to graphene, the $MoSe_2$ monolayer is either physisorbed or chemisorbed on metal surfaces[46,47]. Since Au is an *s*-electron metal with fully occupied *d*-orbitals, $MoSe_2$ weakly interacts with the Au (111) surface. In spite of the weak interaction, the potential drop at the Au|$MoSe_2$ interface, and hence ΔW, is quite sensitive to the interface separation c_d. The calculated values for ΔW increases with decreasing separation of the $MoSe_2$ monolayer from the Au (111) surface, e.g. for c_d equal to 6 Å and 3 Å, ΔW is found to be 0.06 eV and 0.63 eV, respectively. This behavior is attributed to the well known push back effect originating from the Pauli repulsion[48–53]. Even if the bonding at the interface is weak, the Pauli exchange interaction between the $MoSe_2$ monolayer and the surface can significantly affect the charge density distribution at the interface and pushes back some amount of the charge density towards the surface, which lowers *W* of the pristine metal surface. Therefore, a smaller separation leads to an increased interaction and distortion of charge density distribution at the interface, and hence gives rise to a larger ΔW and a smaller *W* as compared to the pristine Au surface, see Table 1 for a summary of *W* and ΔW values as a function of c_d. The electron localization function (ELF) plots shown in Fig. 3 clearly demonstrate the mentioned push back effect. As seen in Fig. 3,

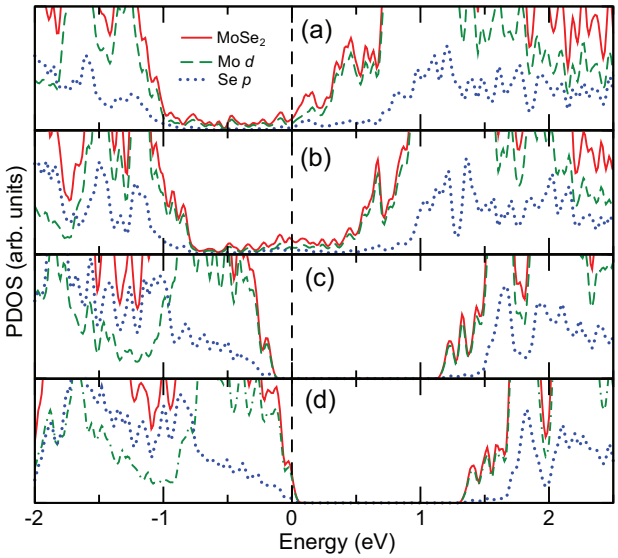

Fig. 5 (Color online) The calculated partial density of states (PDOS) for the $MoSe_2$ monolayer. PDOS of $MoSe_2$-Au(111) is given for different c_d values: (a) 2.7 Å, (b) 3 Å, and (c) 6 Å. The PDOS for the Au|SCF_3|$MoSe_2$ system is shown in (d). Vertical dashed line denotes the position of the Fermi level.

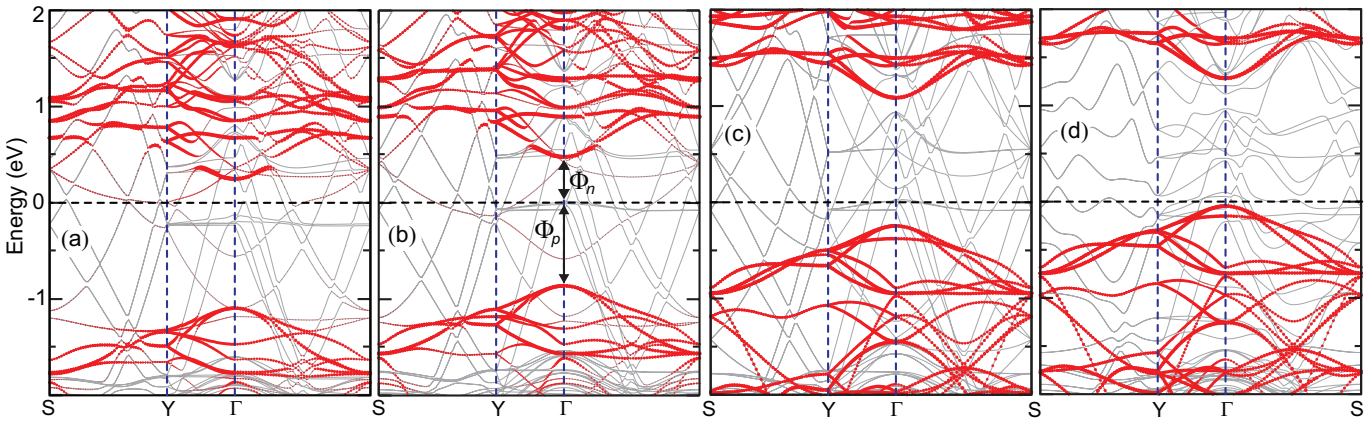

Fig. 2 (Color online) The calculated band structure in a rectangular Brillouin zone for the $MoSe_2$ monolayer contacted to the pristine Au surface with physical separation of (a) 2.7 Å, (b) 3 Å, (c) 6 Å and (d) SAM (SCF_3) modified Au surface. The filled red circles represent the projected band structure for the $MoSe_2$ monolayer. The gray curves show the energy bands for the Au surface and the SAM layer. Horizontal black dashed line denotes the Fermi level. Φ_p and Φ_n are the Schottky barrier heights for holes and electrons, respectively.

the charge density around the bottom layer Se atoms is significantly perturbed at c_d = 2.7 and 3 Å. However, for c_d = 6 Å, the charge density at the bottom and top layer Se atoms becomes symmetric with respect to Mo layer. The separation also leads to a notable change in the charge density around the Au atoms, particularly at the top where Se atoms reside. As seen in the figure, the charge density around the Au atoms having an egg like shape for c_d = 6 Å is substantially modified as the $MoSe_2$ monolayer approaching to the Au surface.

The effect of c_d on the electronic structure is systematically investigated. Fig. 2 shows the calculated band structures for the adsorbed $MoSe_2$ monolayer on pristine and SAM modified Au surfaces. The physical separation and the pre-adsorbed molecules both have a significant impact on the electronic structure at the interface. In the absence of SAM, i.e. for Au|$MoSe_2$, the Fermi level shifts towards the valence band edge as c_d increases. As seen in Table 1 and Fig. 4, for c_d=3 Å (which is the equilibrium separation when the van der Waals interaction is not taken into account), the Fermi level lies within the band gap of $MoSe_2$ and therefore rather high Schottky barrier heights are obtained for both electrons and holes; 0.48 and 0.86 eV, respectively. However, for c_d=6 Å, the Schottky barrier height for holes drops to 0.24 eV. Here, c_d=2.7 Å, which is the equilibrium separation when the van der Waals interactions is included, is also considered, and the Schottky barrier height is predicted to be 0.25 eV for electrons and 1.09 eV for holes. Our results clearly indicates that the Schottky barrier heights can be significantly tuned by adjusting the interface separation between the Au surface and the $MoSe_2$ monolayer, see Fig. 4.

In addition, the type of doping of the $MoSe_2$ monolayer can be modulated by changing the separation c_d. In contrast to

Table 1 The physical separation, c_d, between the top layer of pristine or SAM covered metal surface and bottom Se layer of $MoSe_2$ monolayer, work function (W), work function change (ΔW) with respect to the pristine metal surface, Schottky barrier height (which is the difference between the Fermi level and either the valence band edge or the conduction band edge of the $MoSe_2$ monolayer) for holes (Φ_p) and electrons (Φ_n) in units of eV. For the Au|$MoSe_2$ structure, we present results for three different physical separations (c_d), namely 2.7, 3, and 6 Å. A negative Schottky barrier height means that the Fermi level appears within either the valence or the conduction band of the $MoSe_2$ monolayer.

System	c_d (Å)	W	ΔW	Φ_p	Φ_n
Au		5.23			
Au|$MoSe_2$	2.70	4.50	-0.73	1.09	0.25
	3.00	4.60	-0.63	0.86	0.48
	6.00	5.17	-0.06	0.24	1.09
Au|SCF_3		5.81	0.58		
Au|SCF_3|$MoSe_2$	2.68	5.40	0.17	0.042	1.29
Au|$SC_2H_2F_3$		6.13	0.90		
Au|$SC_2H_2F_3$|$MoSe_2$	2.84	5.34	0.11	0.036	1.29
Au|SCH_3		4.09	-1.14		
Au|SCH_3|$MoSe_2$	2.06	4.35	-0.87	1.11	0.21
Au|$SCNH_4$		3.81	-1.42		
Au|$SCNH_4$|$MoSe_2$	2.54	4.16	-1.07	1.31	0.02
Sc		3.45			
Sc|$MoSe_2$	2.01	4.20	0.75	1.49	0.35
Sc|SCH_3		2.92	-0.53		
Sc|SCH_3|$MoSe_2$	2.93	3.82	0.37	1.48	-0.024

the *p*-type characteristics at c_d=6 Å, *n*-type behavior emerges for c_d=3 Å, the equilibrium distance predicted by GGA. Such behavior can be ascribed to the push back effect especially for the weakly interacting metal-TMD systems. Previously, for a similar system, Au-contacted MoS_2, *n*-type behavior with a high contact resistance instead of *p*-type behavior[14,54] was predicted as parallel with our calculations.

In order to shed more light on the electronic properties at the interfaces, we calculated the partial density of states (PDOS). Comparing the PDOS for different c_d values, the effect of the increased interaction of $MoSe_2$ with the Au surface can be seen in Fig. 5. For short separations, for instance at c_d =2.7 Å, we observe a hybridization of surface and $MoSe_2$ states, giving rise to gap states within the band gap of the supported $MoSe_2$ monolayer. Our PDOS calculations, shown in Figs. 5(a) and (b), demonstrate that these gap states originate mainly from Mo *d*-orbitals with a small contribution from Se *p*-orbitals, which may result in a partial Fermi level pinning that has been recently shown for both low (such as Al) and high work function metals (such as Pt)[55]. Increasing the physical separation between the Au surface and the $MoSe_2$ monolayer leads to a smaller modification of the metal work function and weakens the interface hybridization thereby resulting in fewer gap states.

Following the Au|$MoSe_2$ structure, the Au|SCF_3|$MoSe_2$ system shown in Fig. 1(c) is systematically investigated. In the GGA + vdW optimized structure, the distance between two planes formed by the topmost F atoms of the SCF_3 molecules and the lowermost Se atoms of the $MoSe_2$ monolayer is 2.68 Å. Since the F and Se atoms carry a negative net charge, they avoid each other and the interatomic distance between the F and Se atoms becomes on average 3.2 Å. While GGA-PBE functional does not result in a binding between Au|SCF_3 and $MoSe_2$ systems, we obtain a binding energy of about 0.1 eV (per $MoSe_2$ unit) in GGA + vdW. Next, we focus on the electronic structure of this three layer structure composed of the Au surface, SAM and $MoSe_2$ monolayer. The calculated band structure and PDOS demonstrates *p*-type characteristics for the adsorbed $MoSe_2$ monolayer as seen in Fig. 2(d) and Fig. 5(d). In other words, the Fermi level appears very close to the top of the valence band edge, indicating a very strong *p*-type doping of the $MoSe_2$ monolayer. The Schottky barrier height is also calculated and predicted to be 0.042 eV. At finite temperatures, thermionic emission may obscure such a small Schottky barrier height, and hence the contact of the $MoSe_2$ monolayer with the SAM modified Au surface may exhibit Ohmic behavior. Consistent with our results, Qui *et al.*[56] showed recently that while bilayer MoS_2 FET with titanium contact displays an *n*-type Ohmic behavior at room temperature, a Schottky type characteristic with a barrier height of 65 meV emerges at low temperatures. The effect of the insertion of SAM on the electronic structure can be explained by the appearance of a dipole layer at the interface. The dipole layer results in a potential step at the interface, which effectively changes the work function of the metal surface. In the Au case, the work function of the pristine surface increases from 5.23 eV to 5.81 eV. The presence of the dipole layer between the Au (111) surface and the $MoSe_2$ monolayer significantly alters the energy level alignment at the interface. Similar to the finding of Refs. 46,47, we observe an *p*-type doping of $MoSe_2$ by tuning the position of the Fermi level within the band gap of the $MoSe_2$ monolayer. Furthermore, the gap states, which are considered as one of the main reason for Fermi level pinning, disappears upon the deposition of SAM. Notice that PDOS of $MoSe_2$ on the Au(111) surface for c_d=6 Å is quite similar to that of $MoSe_2$ on the SAM modified surface, see Fig. 2(c) and Fig. 2(d).

Here, a natural question may arise: what happens if one grows SCH_3 molecules on an Au surface? Our calculations reveal that the $MoSe_2$ monolayer exhibits a strong *n*-type behavior when being placed on a SCH_3 SAM modified Au surface since the SCH_3 SAM lowers the work function of the pristine Au (111) surface from 5.23 eV to 4.09 eV, see Table 1. The calculated Schottky barrier heights (i.e. Φ_p and Φ_n) becomes 1.11 eV for holes and 0.21 eV for electrons. This result suggests that the doping characteristic of the $MoSe_2$ monolayer (i.e. *n*- or *p*-type) can be easily tuned by using an appropriate SAM regardless of how large the work function of the metal surface is.

As mentioned previously, one can find ample amount of different SAMs with diverse physical and chemical properties that can be tuned by changing chemical composition and length of the SAM. However, SAMs with longer chain might result in an exponential decrease of the tunneling current due to the increase in the separation between $MoSe_2$ monolayer and metal. In order to further investigate the effect of length of SAM, we also performed calculations for the longer chain alkanethiols, including $SC_2H_2F_3$, $SC_4H_6F_3$ and $SC_5H_8F_3$ on an Au surface. For the sake of brevity, in Table 1, we present the results only for $SC_2H_2F_3$. As mentioned in the previous works[28,30,32], depending on the length of the molecule, the work function of the Au surface covered with alkanethiols based SAMs exhibits an even-odd oscillation. ΔW for SAM with molecules having odd number of C atoms is smaller than that for SAM with molecules having even number of C atoms. While ΔW is 0.6 eV in the former case, it becomes 0.9 eV for the latter case. Here ΔW is calculated with respect to the pristine Au surface. Since all F atoms in the terminal group of the SAM molecules point upwards, the intrinsic dipole is much larger in the latter case, resulting in a larger work function change. In addition, the change in the Schottky barrier heights is of order of $\pm$10 meV.

In addition to the longer chain alkanethiols we also consider -NH_2 unit as a terminal group instead of -CH_3 or -CF_3.

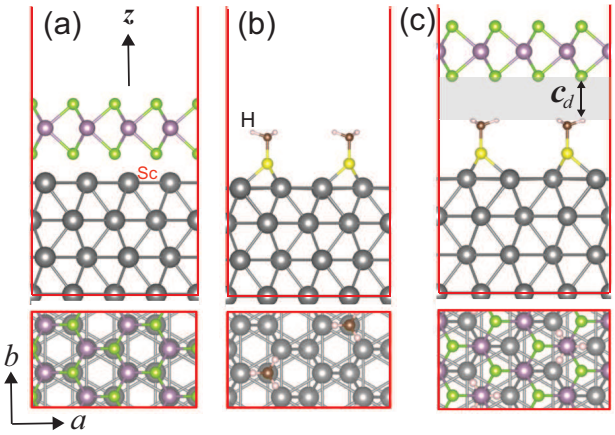

Fig. 6 (Color online) The optimized lowest energy structures from different perspectives: (a) $MoSe_2$ monolayer on a Sc (0001) surface, (b) Sc surface with SCH_3 SAM, and (c) $MoSe_2$ monolayer on the SAM covered Sc surface.

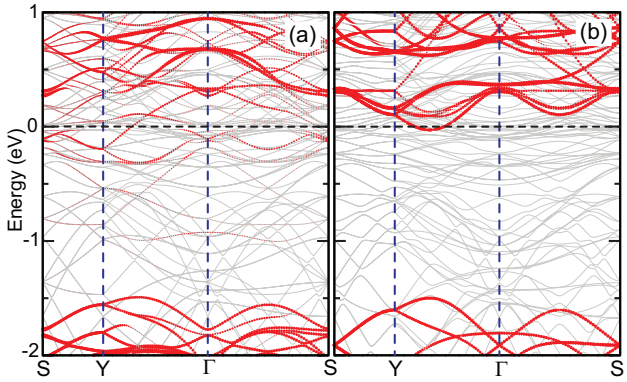

Fig. 7 (Color online) Band structure of the $MoSe_2$ monolayer contacted to: (a) pristine and (b) SAM (SCH_3) modified Sc surfaces. The filled red circles represent the projected band structure for the $MoSe_2$ monolayer. The gray curves show the bands for the Au surface and the SAM layer. Horizontal black dashed line denotes the Fermi level.

As seen in Table 1, it is found that the adsorption of $SCNH_4$ SAM on the Au (111) surface decreases the workfunction of the pristine surface from 5.23 eV to 3.81 eV. Since $SCNH_4$ SAM significantly lowers the work function of the Au surface, one expects an *n*-type doping of $MoSe_2$ monolayer. Indeed, the calculated Schottky barrier heights are found to be 0.02 eV for electrons and 1.31 eV for holes, resulting in a strong *n*-type behavior. As presented in Table 1, the Schottky barrier is calculated as 0.21 eV for electrons in Au|SCH_3|$MoSe_2$ system. These results clearly show that barrier heights can be tuned by changing the terminal group of SAM molecules. As shown experimentally, at reasonable high temperatures (for instance at room temperature), the contact type for $SCNH_4$ SAM is certainly expected to switch from Schotkky to Ohmic as a result of thermoionic emissions[56].

3.2 Sc|SCH_3|$MoSe_2$

Next, the effect of SAM on a low work function metal is studied by replacing the Au surface by Sc, see Fig. 6 for the optimized structures. The Sc electrode has been shown recently to be a better contact with thin MoS_2 flakes, resulting in a lower contact resistance and higher carrier injection as compared to Ti, Ni, and Pt[18]. In contrast to Au, $MoSe_2$ interacts strongly with the pristine Sc (0001) surface with a binding energy of 1 eV per surface atom. The adsorption of the $MoSe_2$ monolayer on the metal surface increases the work function of the pristine Sc surface from 3.45 to 4.20 eV, implying a partial charge transfer from the Sc surface to the $MoSe_2$ monolayer. Adversely the work function of the Sc surface decreases with $\Delta W = 0.53$ eV upon adsorption of SAM since the normal component of the dipole associated with the SCH_3 molecule is opposite to that of the SCF_3 molecule. The binding structure of the SCH_3 molecules on the Sc surface is different as compared to that on the Au surface[45]. H atoms of the SCH_3 molecule prefer to stay within the same plane parallel to the metal surface, see Fig.6. We identified two different growth structures of the $MoSe_2$ monolayer on the SAM modified Sc surface with almost identical electronic properties. While, in the first structure, Se atoms sit at the top of the H atoms, SCH_3 molecules are rotated by 60° with respect to the first structure. The energy difference between these growth configurations is just 10 meV in favor of the second structure. In contrast to Au|SAM|$MoSe_2$, the work function makes a significant increase when $MoSe_2$ is placed on the SAM modified Sc surface, which can be attributed to a spontaneous charge transfer from the Sc surface to the $MoSe_2$ monolayer across the SAM layer.

Fig. 8 shows PDOS for the adsorbed $MoSe_2$ on the pristine and the SAM modified Sc (0001) surfaces. Although the strong interaction leads to a remarkable hybridization of the Sc surface and the $MoSe_2$ states to a certain extent, the valence and conduction bands of the adsorbed $MoSe_2$ monolayer can be still identified, see Fig. 8(a). For Sc|$MoSe_2$, even though there is no direct interaction between the Sc and Mo atoms, the main contribution to the gap states comes from Mo the *d*-orbitals. Similar to the findings of Gong *et al.*[55], Se atoms mediate the interaction between the surface and the Mo atoms. The strong Sc-Se interaction weakens the Se-Mo bonding and hence alters the electronic structure of the adsorbed $MoSe_2$ monolayer. Indeed, the band edges of $MoSe_2$ is mainly composed of Mo *d*-orbitals which spill into the band gap of $MoSe_2$ as a result of the strong interaction thereby causing the formation of gap states. The band structure of the $MoSe_2$ monolayer

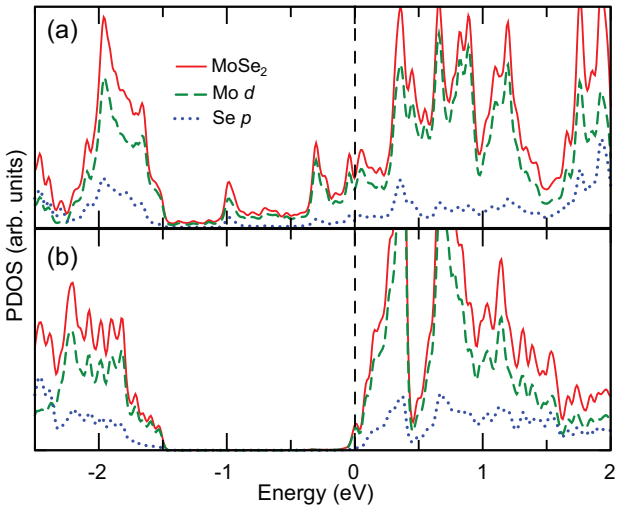

Fig. 8 (Color online) The calculated partial density of states (PDOS) for the $MoSe_2$ monolayer: (a) PDOS of Sc(0001)|$MoSe_2$, and (b) PDOS for the Sc|SCH_3 |$MoSe_2$ system. Vertical dashed line denotes the position of the Fermi level.

placed on the pristine Sc surface confirms that the conduction band of $MoSe_2$ significantly broadens and spreads into the band gap of $MoSe_2$, see Fig. 7(a).

One of the main differences between the Au|$MoSe_2$ and Sc|$MoSe_2$ interfaces is that the latter displays a much higher density of states at and near the Fermi level since the interaction of the $MoSe_2$ monolayer with the Sc surface is much stronger. Consistent with a previous experimental study reporting *n*-type characteristics in a MoS_2 based FET, the Fermi level lies very close to the conduction band edge of the $MoSe_2$ monolayer. Furthermore, the metal/MoS_2 interface was shown to be strongly affected by the Fermi level pinning close to the conduction band edge of MoS_2. The existence of interface states within the band gap of $MoSe_2$ plays a key role in the Fermi level pinning. The insertion of a SAM between a metal surface and a TMD monolayer completely eliminates the pinning of the Fermi level close to the conduction band edge by removing the band gap states. Since the adsorption of SAM decreases the work function of the Sc surface, the Fermi level shifts towards the conduction band of $MoSe_2$. In spite of the presence of a large Schottky barrier with a value of 0.35 eV for electrons at the Sc-$MoSe_2$ interface, a strong *n*-type behavior with a Schottky barrier height of -0.024 eV is achieved for the Sc|SCH_3|$MoSe_2$ system, see Fig. 7(b). A negative value means that the Fermi level lies within the conduction band of $MoSe_2$. Thus the contact may switches from Schottky to Ohmic, which results in a very low contact resistance, an increased carrier density, and a high carrier injection efficiency across the interface. Similar to the Au case described above, the doping of the $MoSe_2$ monolayer has an electrostatic origin, that is nothing else then the substantial potential step originated from the interface dipole layer which lowers the work function of the metal surface, and consequently causes the *n*-type doping of $MoSe_2$.

Semi-local exchange correlation functionals (ECF) usually misestimates the energy level alignment between the weakly interacting systems. In order to check the effect of ECF on the position of the Fermi level and hence the energy level alignment at the interface, we also performed HSE06 calculations. Although the choice of ECF has a remarkable effect on the band gap of the $MoSe_2$ monolayer, the Fermi level is predicted at nearly the same position relative to the valence band edge in the Au|SCF_3|$MoSe_2$ system and conduction band edge in the Sc|SCH_3|$MoSe_2$ system in GGA and HSE06 calculations. The band gap (i.e. difference between the top of the valence band and bottom of the conduction band) of the adsorbed $MoSe_2$ is calculated as 1.72 eV in HSE06 calculations as compared to 1.33 eV in GGA calculations. The Schottky barrier for electrons (holes) is found to be about $\sim$ -0.01 eV ($\sim$ 0.03 eV) in the Sc|SCH_3|$MoSe_2$ (Au|SCF_3|$MoSe_2$) system. Therefore, these results show that the calculated band gap and the Schottky barrier for carriers are robust against the choice of the exchange-correlation functionals.

The results obtained in this study clearly demonstrate that *n*- or *p*- doping in TMDs can be tuned by interface engineering. Very recently, it was shown that the conductivity, field effect mobility, and optical properties of MoS_2 monolayers can be effectively enhanced or modulated by using an appropriate SAM[26]. By calculating the work function change, i.e. the Fermi level shift, of $MoSe_2$ on pristine and SAM modified metal surfaces, we find that SAMs can affect the carrier distribution and charge transfer process between the $MoSe_2$ monolayer and the metal substrate by lowering the Schottky barrier height. Exploring the modulation of the work function of the metal surface by SAMs is essential to tune the energy level alignment at the contacts and control the contact barriers. Since organic molecules are promising candidates for flexible electronics, the engagement of the potentials of SAM and TMDs encourages the use of TMDs in novel flexible electronics applications.

4 Conclusion

We showed that the electronic properties of $MoSe_2$ can be modified by manipulating its interaction with metal electrodes using a self-assembled monolayer of polar molecules. Furthermore, the *n*- or *p*-type characteristic of $MoSe_2$ can be significantly tuned by inserting different SAM monolayers. We obtained much lower Schottky barrier heights for the SAM modified surfaces as compared to the pristine surfaces which can be even reduced to Ohmic. Our results show that SAMs have potential to be used as a buffer layer instead of oxides to

tune the work function of metal surfaces and the energy level alignment between a metal electrode and a TMD monolayer.

Part of this work is supported by the Flemish Science Foundation (FWO-VI) and the Methusalem foundation of the Flemish Government. Computational resources were provided by TUBITAK ULAKBIM, High Performance and Grid Computing Center (TR-Grid e-Infrastructure). D. C. is supported by a FWO Pegasus-short Marie Curie Fellowship. C. S. acknowledges the support from Scientific and Technological Research Council of Turkey (TUBITAK 113F096), Anadolu University (BAP-1306F281, -1404F158) and Turkish Academy of Science (TUBA).

References

1 K. S. Novoselov, A. K. Geim, S. V. Morozov, D. Jiang, S. C. Dubonos, I. V. Grigorieva and A. A. Firsov, *Science*, 2004, **306**, 666.
2 K. S. Novoselov and A. K. Geim, *Nat. Mater.*, 2007, **6**, 183.
3 A. H. Castro Neto, F. Guinea, N. M. R. Peres, K. S. Novoselov and A. K. Geim, *Rev. Mod. Phys.*, 2009, **81**, 109–162.
4 S. Das Sarma, S. Adam, E. H. Hwang and E. Rossi, *Rev. Mod. Phys.*, 2011, **83**, 407–470.
5 K. F. Mak, C. Lee, J. Hone, J. Shan and T. F. Heinz, *Phys. Rev. Lett.*, 2010, **105**, 136805.
6 C. Ataca, H. Şahin and S. Ciraci, *J. Phys. Chem. C*, 2012, **116**, 8983–8999.
7 Q. H. Wang, K. Kalantar-Zadeh, A. Kis, J. N. Coleman and M. S. Strano, *Nat. Nanotechnol.*, 2012, **7**, 699–712.
8 X. Song, J. Hu and H. Zeng, *J. Mater. Chem. C*, 2013, **1**, 2952–2969.
9 M. Xu, T. Liang, M. Shi and H. Chen, *Chem. Rev.*, 2013, **113**, 3766–3798.
10 X. Huang, Z. Zeng and H. Zhang, *Chem. Soc. Rev.*, 2013, **42**, 1934–1946.
11 M. Chhowalla, H. S. Shin, G. Eda, L.-J. Li, K. P. Loh and H. Zhang, *Nat. Chem.*, 2013, **5**, 263–275.
12 D. Jariwala, V. K. Sangwan, L. J. Lauhon, T. J. Marks and M. C. Hersam, *ACS Nano*, 2014, **8**, 1102–1120.
13 H. Wang, H. Feng and J. Li, *Small*, 2014, n/a–n/a.
14 B. Radisavljevic, A. Radenovic, J. Brivio, V. Giacometti and A. Kis, *Nat. Nanotechnol.*, 2011, **6**, 147.
15 S. Larentis, B. Fallahazad and E. Tutuc, *Appl. Phys. Lett.*, 2012, **101**, 223104.
16 W. Liu, J. Kang, D. Sarkar, Y. Khatami, D. Jena and K. Banerjee, *Nano Lett.*, 2013, **13**, 1983–1990.
17 A. Dankert, L. Langouche, M. V. Kamalakar and S. P. Dash, *ACS Nano*, 2014, **8**, 476–482.
18 S. Das, H.-Y. Chen, A. V. Penumatcha and J. Appenzeller, *Nano Lett.*, 2013, **13**, 100–105.
19 W. Chen, E. J. G. Santos, W. Zhu, E. Kaxiras and Z. Zhang, *Nano Lett.*, 2013, **13**, 509–514.
20 W. Liu, J. Kang, D. Sarkar, Y. Khatami, D. Jena and K. Banerjee, *Nano Lett.*, 2013, **13**, 1983–1990.
21 J. Kang, W. Liu and K. Banerjee, *Appl. Phys. Lett.*, 2014, **104**, 093106.
22 I. Popov, G. Seifert and D. Tománek, *Phys. Rev. Lett.*, 2012, **108**, 156802.
23 J. Kang, D. Sarkar, W. Liu, D. Jena and K. Banerjee, 2012, 17.4.1–17.4.4.
24 J.-R. Chen, P. M. Odenthal, A. G. Swartz, G. C. Floyd, H. Wen, K. Y. Luo and R. K. Kawakami, *Nano Lett.*, 2013, **13**, 3106–3110.
25 A. Dankert, L. Langouche, M. V. Kamalakar and S. P. Dash, *ACS Nano*, 2014, **8**, 476–482.
26 Y. Li, C.-Y. Xu, P. Hu and L. Zhen, *ACS Nano*, 2013, **7**, 7795–7804.
27 A. Ulman, *Chem. Rev.*, 1996, **96**, 1533–1554.
28 J. C. Love, L. A. Estroff, J. K. Kriebel, R. G. Nuzzo and G. M. Whitesides, *Chem. Rev.*, 2005, **105**, 1103–1170.
29 G. Heimel, L. Romaner, J.-L. Brédas and E. Zojer, *Phys. Rev. Lett.*, 2006, **96**, 196806.
30 P. C. Rusu and G. Brocks, *J. Phys. Chem. B*, 2006, **110**, 22628–22634.
31 Q. Sun and A. Selloni, *J. Phys. Chem.. A*, 2006, **110**, 11396–11400.
32 P. C. Rusu and G. Brocks, *Phys. Rev. B*, 2006, **74**, 073414.
33 G. Heimel, L. Romaner, E. Zojer and J.-L. Brédas, *Nano Lett.*, 2007, **7**, 932–940.
34 D. Cornil, Y. Olivier, V. Geskin and J. Cornil, *Adv. Funct. Mater.*, 2007, **17**, 1143–1148.
35 B. Chamlagain, Q. Li, N. J. Ghimire, H.-J. Chuang, M. M. Perera, H. Tu, Y. Xu, M. Pan, D. Xaio, J. Yan, D. Mandrus and Z. Zhou, *ACS Nano*, 2014, **8**, 5079–5088.
36 G. Kresse and J. Furthmüller, *Phys. Rev. B*, 1996, **54**, 11169–11186.
37 G. Kresse and D. Joubert, *Phys. Rev. B*, 1999, **59**, 1758–1775.
38 G. Kresse and J. Hafner, *Phys. Rev. B*, 1993, **47**, 558–561.
39 H. J. Monkhorst and J. D. Pack, *Phys. Rev. B*, 1976, **13**, 5188–5192.
40 S. Grimme, *J. Comput. Chem.*, 2006, **27**, 1787–1799.
41 M. Amft, S. Lebègue, O. Eriksson and N. V. Skorodumova, *J. Phys.: Condens. Matter*, 2011, **23**, 395001.
42 J. Heyd, G. E. Scuseria and M. Ernzerhof, *J. Chem. Phys.*, 2003, **118**, 8207–8215.
43 J. Paier, M. Marsman, K. Hummer, G. Kresse, I. C. Gerber and J. G. Ángyán, *J. Chem. Phys.*, 2006, **125**, 249901.
44 J. Heyd, G. E. Scuseria and M. Ernzerhof, *J. Chem. Phys.*, 2006, **124**, 219906.
45 P. C. Rusu and G. Brocks, *J. Phys. Chem. B*, 2006, **110**, 22628–22634.
46 G. Giovannetti, P. A. Khomyakov, G. Brocks, V. M. Karpan, J. van den Brink and P. J. Kelly, *Phys. Rev. Lett.*, 2008, **101**, 026803.
47 P. A. Khomyakov, G. Giovannetti, P. C. Rusu, G. Brocks, J. van den Brink and P. J. Kelly, *Phys. Rev. B*, 2009, **79**, 195425.
48 N. D. Lang, *Phys. Rev. Lett.*, 1981, **46**, 842–845.
49 P. S. Bagus, D. Käfer, G. Witte and C. Wöll, *Phys. Rev. Lett.*, 2008, **100**, 126101.
50 M. Schwoerer and H. C. Wolf, *H. C. Wolf*, WILEY-VCH, 2006.
51 H. Ishii, K. Sugiyama, E. Ito and K. Seki, *Advanced Materials*, 1999, **11**, 605–625.
52 A. Kahn, N. Koch and W. Gao, *Journal of Polymer Science Part B: Polymer Physics*, 2003, **41**, 2529–2548.
53 P. S. Bagus, V. Staemmler and C. Wöll, *Phys. Rev. Lett.*, 2002, **89**, 096104.
54 M. Fontana, T. Deppe, A. K. Boyd, M. Rinzan, A. Y. Liu, M. Paranjape and P. Barbara, *Sci. Rep.*, 2013, **3**, 1634.
55 C. Gong, L. Colombo, R. M. Wallace and K. Cho, *Nano Lett.*, 2014, **14**, 1714–1720.
56 H. Qiu, L. Pan, Z. Yao, J. Li, Y. Shi and X. Wang, *Appl. Phys. Lett.*, 2012, **100**, 123104.